Towards effective analysis of large grain boundary data sets

K Glowinski and A Morawiec

Instiute of Metallurgy and Materials Science, Polish Academy of Sciences, Kraków, Poland

E-mail: kglowinski@ymail.com

Abstract. Grain boundaries affect properties of polycrystals. Novel experimental techniques for three-dimensional orientation mapping give new opportunities for studies of this influence. Large networks of boundaries can be analyzed based on all five 'macroscopic' boundary parameters. We demonstrate benefits of applying two methods for improving these analyses. The fractions of geometrically special boundaries in ferrite are estimated based on 'approximate' distances to the nearest special boundaries; by using these parameters, the times needed for processing boundary data sets are shortened. Moreover, grain-boundary distributions for nickel are obtained using kernel density estimation; this approach leads to distribution functions more accurate than those obtained based on partition of the space into bins.

1. Introduction

The evolution of experimental techniques for three-dimensional (3-D) microstructure imaging (e.g., automated serial sectioning, X-ray tomography) has made it possible to determine grain misorientations and boundary plane indices (i.e., all five macroscopic boundary parameters) for significant numbers of boundaries (e.g., [1, 2]). This has increased the interest in quantitative characterization of boundary networks (e.g., [3]). However, the boundary studies with five parameters taken into account turn out to be complex compared to those limited solely to grain orientations. Although progress in the development of experimental equipment has been made, acquisition of large 3-D data sets is still cumbersome. It is, therefore, important to analyze the data in a way that is both efficient and does not distort final conclusions. In this note, two practical examples of increasing effectiveness of the analysis are presented. First, the fractions of geometrically special boundaries in ferritic steel are estimated using fast-to-calculate parameters defined in [4] and [5]. These fractions supplement the characterization of the boundary network of this material given in [2]. Then, grain-boundary distributions for pure nickel, already studied in [1], are reconsidered; more accurate and reliable distributions are obtained using an approach based on multivariate kernel density estimation (KDE) [6]. Besides that, a scheme of detailed interpretation of these distributions is suggested.

2. Geometrically special grain boundaries in ferrite

Five-tuples of macroscopic boundary parameters constitute the 5-D boundary space [7]. Crystal and grain-exchange symmetries imply that different 5-tuples may represent the same physical boundary, and all these equivalent representations need to be considered. Differences in geometries of boundaries can be quantified by means of a metric defined in the space: the

Table 1. Area-weighted fractions (assuming the tolerance of 8°) of geometrically special boundaries in ferritic steel. Values in parentheses correspond to 10^7 random boundaries.

Twist	180°-tilt	Symmetric	180°-tilt & symmetric
21.2% (22.0%)	29.3% (21.9%)	2.2% (1.4%)	1.5% (0.7%)

distance between two boundaries minimized over all representations is small (large) if they are similar (distinct). Boundaries of special geometric features, e.g., tilt, twist, symmetric, 180°-tilt boundaries serve as reference points in the boundary space, and general boundaries are characterized by their distances to the nearest reference boundaries. However, calculation of the distances to the nearest special boundaries is complicated and time-consuming. In order to speed up such characterization for large numbers of boundaries, the distances can be replaced by parameters defined in [4] and [5] that are easy to calculate and strongly correlated with the true distances. These 'approximate distances' are used here for estimation of the fractions of geometrically special boundaries in a 3-D network of about $8,300$ boundaries extracted from a ferritic steel sample. For the steel composition and processing history, and for the data acquisition details, see [2]. The boundaries were reconstructed in the form of a triangular mesh using *DREAM.3D* [8] program. In total, there were about 1.4×10^6 triangular boundary segments. Computation of the approximate distances for all segments took about 2 minutes on a 4-core PC whereas obtaining of accurate distances would take about 65 hours. A segment was classified as a twist, symmetric, or 180°-tilt boundary if the approximate distances to the nearest twist, symmetric, and 180°-tilt boundary, respectively, calculated for that segment were below 8°. This limit is determined by the experimental capabilities, cf. [5]. With such resolution, tilt boundaries in materials with cubic $m\bar{3}m$ crystal symmetry are indistinguishable [4]. The fractions of other special boundaries obtained for ferrite are compared to those calculated for random boundaries in Tab. 1. Only the percentages for symmetric boundaries and 180°-tilt boundaries differ significantly from those corresponding to the random data. From the distributions (Fig. 1) of the approximate distances α_S and α_I to the nearest symmetric boundaries and 180°-tilt boundaries, respectively, it follows that, indeed, near-symmetric boundaries (i.e., those with α_S close to zero) and near-180°-tilt boundaries (those with small α_I) are over-represented. It was reported in [2] that in the investigated steel, there is a high population of the $\Sigma 3/(\bar{2}11)$ – simultaneously symmetric and 180°-tilt – boundaries. Therefore, it is interesting to identify the largest subgroups of all symmetric boundaries and 180°-tilt boundaries. This is done based on the distributions of α_S and α_I, respectively, obtained for the complete data set and its subsets (Fig. 1). It is inferred that the contributions of near-$\Sigma 3$ boundaries to both symmetric and 180°-tilt boundaries are minor, while the dominant inputs are those of small-angle boundaries.

3. Distributions of grain boundaries in nickel

Populations of boundaries as functions of the five macroscopic parameters are the primary tool for studying 3-D boundary networks. The populations are conventionally given as multiples of random distributions (MRD) and depicted in the form of 2-D sections for fixed misorientations and varying boundary planes. For instance, sections for the $\Sigma 3$, $\Sigma 5$, $\Sigma 7$, and $\Sigma 9$ misorientations obtained for a data set collected from a pure nickel sample were shown in [1]. Those distributions were computed using a method based on partition of the boundary space into equivolume bins and counting boundary segments that fall into the bins [3]. However, as pointed out in [6], the elongated dimensions of some bins, averaging over equivalent bins, and poor correspondence between bin sizes and experimental resolutions lead to artifacts complicating interpretation of the resulting functions.

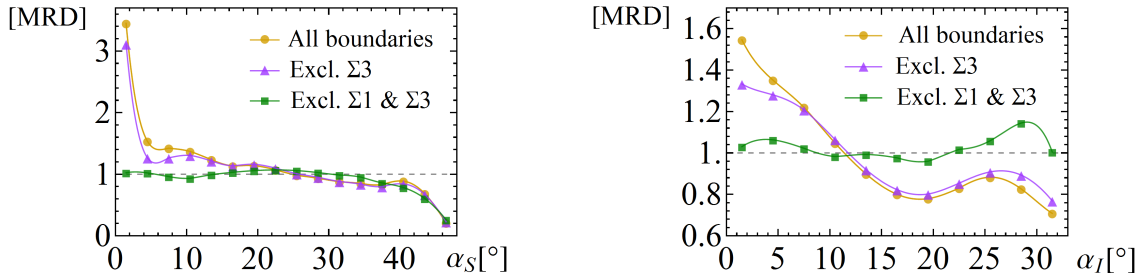

Figure 1. Distributions (in MRD – multiples of random distributions) of the approximate distances α_S and α_I to the nearest symmetric and 180°-tilt boundaries, respectively, computed for the data set of ferrite and its subsets. In the first subset, Σ3 boundaries (according to Brandon criterion) are excluded. The second subset does not contain Σ1 and Σ3 boundaries. (Σ1 boundaries have misorientation angles less than 15° and – due to data clean-up – greater than 5°.) The removed boundaries constitute 7.5% and 29.4% of the complete data, respectively.

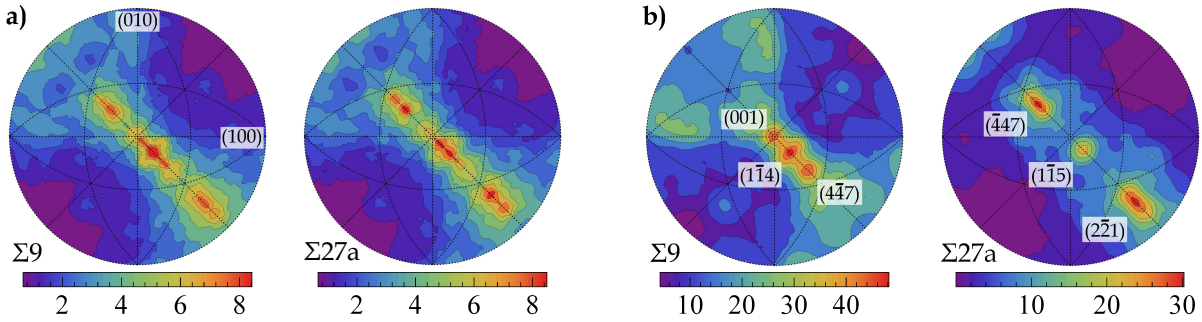

Figure 2. Populations (in multiples of random distributions) of Σ9 and Σ27*a* boundaries in nickel as functions of boundary planes (plotted in stereographic projections) obtained using (a) partition into "10°-bins", and (b) the KDE-based method with $\rho_m = 3°$, $\rho_p = 7°$.

Therefore, the nickel data are reanalyzed. This time the boundary distributions were obtained using a newly developed KDE-based approach that is free from the deficiencies of the partition-based method [6]. Surfaces of about 3,500 boundaries were reconstructed in *DREAM.3D*. Formally, the boundary space is a Cartesian product of the misorientation and boundary-normal subspaces. For computational reasons and because of considerably different resolutions in determinination of misorientation and boundary-plane parameters, it is convenient to use a separate metric in each subspace. First, boundaries with misorientations located not farther from the fixed misorientation than a limiting distance ρ_m are selected. Then, the distribution is probed at evenly distributed normal directions, and boundaries whose normals deviate from a given direction by less than ρ_p are counted. The radii ρ_p and ρ_m were tailored to both resolution and amount of data and set to 3° and 7°, respectively, cf. [6]. The most significant differences between the old method and new approach were observed in the Σ9 and Σ27*a* sections. The sections obtained using partition into typical "10°-bins" overlap and are barely distinguishable (Fig. 2a), whereas those computed using the new approach are clearly separated (Fig. 2b). Moreover, in the KDE-based method, statistical errors of the distributions (thus, their reliability) can be directly evaluated using the formula $\varepsilon \approx (fnv)^{1/2}$ [6]; ε is the relative error of the function at a given point, f is the value of the function at that point, n stands for the number of grain boundaries in the considered network, and v denotes the volume restricted by ρ_m and ρ_p. For instance, the heights of the peaks at the $\Sigma27a/(\bar{4}47)$ and $\Sigma27a/(2\bar{2}1)$ boundaries are

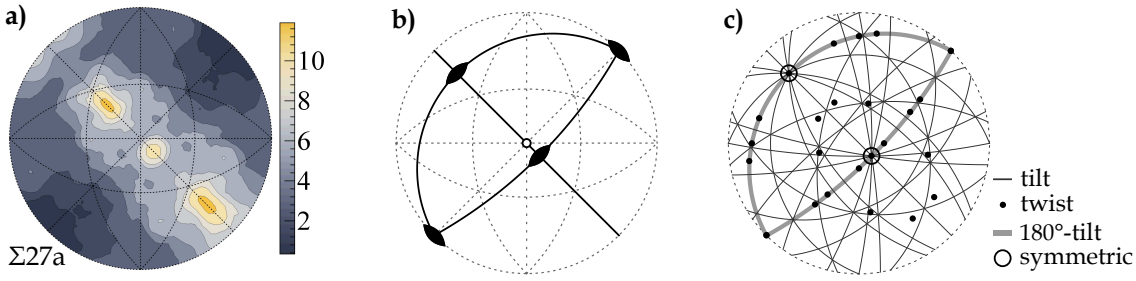

Figure 3. (a) Statistical errors of the distribution for the $\Sigma 27a$ misorientation shown in Fig. 2b. The errors are given as multiples of a random distribution. (b) Symmetries of the $\Sigma 27a$ section. (c) Locations of geometrically special boundaries for the $\Sigma 27a$ misorientation.

20 MRD and the corresponding errors are ±12 MRD. These maxima are higher than those in the sections obtained based on the bins because the volume of the space determined by $\rho_m = 3°$, $\rho_m = 7°$ (used in normalization of the distributions) is about 2 times smaller than the volume of "10°-bins". Moreover, averaging over many bins (thus, flattening of the distributions) was eliminated. Symmetry axes and mirror lines of the $\Sigma 27a$ section are shown in Fig. 3b, cf. [9]. This figure reveals, in particular, that the maxima at the $(\bar{4}47)$ and $(2\bar{2}1)$ poles are actually related to the same physical boundaries. A diagram containing the locations of all tilt, twist, symmetric, and 180°-tilt boundaries with the $\Sigma 27a$ misorientation is presented in Fig. 3c. This map indicates that the peak at the $\Sigma 27a/(2\bar{2}1)$ boundary lies at the intersection of three tilt zones – it has three distinct tilt axes.

4. Final remarks

The recently developed methods which facilitate studies of grain-boundary networks were applied to analysis of boundaries in two metals. Recognition of geometrically special boundaries is more efficient if the accurate distances to the nearest special boundaries are substituted by their approximations. Based on distributions of these parameters, it is concluded that symmetric boundaries and 180°-tilt boundaries are over-represented in the ferrite sample, but majority of them are small-angle boundaries. Most artifacts in grain-boundary distributions are reduced if KDE is used instead of the partition-based approach. In particular, the new method allows for detailed interpretation of the $\Sigma 9$ and $\Sigma 27a$ sections obtained for pure nickel as they do not overlap (as the overlap occurring in the conventional method with typical "10°-bins" is avoided).

Acknowledgments

The authors are grateful to Professor Gregory S. Rohrer (of Carnegie Mellon University) for permission to use the ferrite and nickel data. The work of K.G. was supported by the European Union under the European Social Fund within project No. POKL.04.01.00-00-004/10.

References

[1] Li J, Dillon S J and Rohrer G S 2009 *Acta Mater.* **57** 4304
[2] Beladi H and Rohrer G S 2013 *Acta Mater.* **61** 1404
[3] Saylor D M, Morawiec A and Rohrer G S 2003 *Acta Mater.* **51** 3663
[4] Morawiec A and Glowinski K 2013 *Acta Mater.* **61** 5756
[5] Glowinski K 2014 *J. Appl. Cryst.* **47** 726
[6] Glowinski K and Morawiec A 2014 *Metall. Mater. Trans.* **A45** 3189
[7] Morawiec A 2009 *J. Appl. Cryst.* **42** 783
[8] Groeber M A and Jackson M A 2014 *Integr. Mater. Manuf. Innov.* **3** 5
[9] Patala S and Schuh C A 2013 *Philos. Mag.* **93** 524